ELSEVIER

Contents lists available at ScienceDirect

Journal of Controlled Release

journal homepage: www.elsevier.com/locate/jconrel





Visualisation of drug distribution in skin using correlative optical spectroscopy and mass spectrometry imaging

Natalie A. Belsey ^{a,b,*}, Alex Dexter ^a, Jean-Luc Vorng ^a, Dimitrios Tsikritsis ^a, Chelsea J. Nikula ^a, Teresa Murta ^a, Maria-Vitalia Tiddia ^a, Junting Zhang ^a, Elzbieta Gurdak ^a, Gustavo F. Trindade ^a, Ian S. Gilmore ^a, Leanne Page ^c, Clive S. Roper ^{c,d}, Richard H. Guy ^e, Mila Boncheva Bettex ^{f,**}

- ^a Chemical & Biological Sciences Department, National Physical Laboratory, Teddington TW11 0LW, UK
- ^b School of Chemistry & Chemical Engineering, University of Surrey, Guildford GU2 7XH, UK
- ^c Charles River Laboratories Edinburgh Ltd, Tranent, East Lothian EH33 2NE, UK
- ^d Roper Toxicology Consulting Limited, Edinburgh EH3 6AD, UK
- ^e Department of Life Sciences, University of Bath, BA2 7AY, UK
- f Haleon CH SARL, Route de l'Etraz 2, Case postale 1279, 1260 Nyon 1, Switzerland

ARTICLE INFO

Keywords: Topical drug delivery Diclofenac Skin biodistribution Stimulated Raman scattering microscopy Secondary ion mass spectrometry OrbiSIMS Multiphoton imaging Correlative imaging

ABSTRACT

A correlative methodology for label-free chemical imaging of soft tissue has been developed, combining nonlinear optical spectroscopies and mass spectrometry to achieve sub-micron spatial resolution and critically improved drug detection sensitivity. The approach was applied to visualise the kinetics of drug reservoir formation within human skin following in vitro topical treatment with a commercial diclofenac gel. Non-destructive optical spectroscopic techniques, namely stimulated Raman scattering, second harmonic generation and two photon fluorescence microscopies, were used to provide chemical and structural contrast. The same tissue sections were subsequently analysed by secondary ion mass spectrometry, which offered higher sensitivity for diclofenac detection throughout the epidermis and dermis. A method was developed to combine the optical and mass spectrometric datasets using image registration techniques. The label-free, high-resolution visualisation of tissue structure coupled with sensitive chemical detection offers a powerful method for drug biodistribution studies in the skin that impact directly on topical pharmaceutical product development.

1. Introduction

We developed a new correlative imaging approach that combines nonlinear optical spectroscopies and mass spectroscopy imaging, applied to the same tissue sample for label-free visualisation of both the tissue structure and the distribution of an applied drug.

Raman spectroscopy (RS) is a well-established method for chemical mapping based on the inelastic scattering of light by molecular vibrations [1,2]. RS has been widely used to map drug distribution in cells and tissues [3–5]. However, the data acquisition time required to generate high resolution images is relatively long (several tens of hours), potentially compromising the data integrity for time-sensitive samples; furthermore, depending on the molecular structure of the drug, the method sensitivity can be quite low, especially in deeper tissue layers [3]. Stimulated Raman scattering (SRS) microscopy utilises two lasers

rather than one to stimulate a vibrational mode of interest and to rapidly acquire an image at a single wavenumber at a time [6-8]. This method has successfully been applied to visualise drug distribution in skin [9]. In addition, SRS microscopy can be performed simultaneously to other optical techniques such as second harmonic generation (SHG) and two photon excited fluorescence (TPEF) microscopies for label-free visualisation of the connective tissues, collagen, and elastin, respectively [10-12].

Mass spectrometry imaging (MSI) provides label-free chemical analysis and includes a range of both ambient and high vacuum techniques [13]. Secondary ion mass spectrometry (SIMS) utilises a focused ion beam to sputter the molecules that compose the sample surface. Sputtered molecules are then extracted and identified through a mass analyser with a time-of-flight (ToF) analyser or an Orbitrap analyser [14], more commonly used for organic materials. SIMS offers chemical

^{*} Corresponding author at: Chemical & Biological Sciences Department, National Physical Laboratory, Teddington TW11 0LW, UK.

^{**} Corresponding author at: Haleon CH SARL, Route de l'Etraz 2, Case postale 1279, 1260 Nyon 1, Switzerland. E-mail addresses: natalie.belsey@npl.co.uk (N.A. Belsey), mila.x.bonchevabettex@haleon.com (M.B. Bettex).

analysis with high sensitivity over a large mass range combined with 3D imaging capabilities and high lateral resolution. The recent technological developments of SIMS instrumentation and the implementation of large cluster ion sources have greatly enhanced the sensitivity of the technique making possible the study of diverse sample types [15–17]. SIMS has become well-suited to biological and pharmaceutical applications including the determination of spatial co-localization of pharmaceuticals with biomolecules and drug distribution in single cells and tissues [14,18–23], in addition to molecular characterisation of the skin barrier itself [24,25].

Although both optical spectroscopy and mass spectrometry imaging approaches are powerful when applied individually, they perform differently across important metrics such as chemical sensitivity, specificity, and spatial resolution. It is advantageous, therefore, to combine the complementary information they offer [26]. Previous work involving correlative RS and MSI approaches have been reported; for example, RS has been combined with matrix assisted laser desorption ionisation (MALDI) mass spectrometry imaging [27–29]. MALDI affords much higher chemical specificity, but the combination benefits from the higher spatial resolution achievable with RS. Since MALDI requires the application of a matrix compound, the RS is performed first, or on serial sections [30].

In this work, we correlated the label-free optical imaging modalities SRS, SHG and TPEF with SIMS to achieve a combination of sub-micron spatial resolution and improved chemical sensitivity relative to RS. We developed a workflow, summarised in Fig. 1, allowing analysis of the same (rather than serial) sections of treated skin tissue, thus avoiding artefacts arising from the normal tissue variability. The utility of this new correlative imaging approach was demonstrated in the challenging example of mapping the time course of diclofenac distribution in skin tissue following topical treatment with a commercial product. This task requires a high degree of chemical sensitivity to detect the drug at its therapeutically relevant concentration and in the presence of the formulation excipients (especially within the dermis and subcutis) combined with sufficient spatial resolution to resolve the skin structure. Label-free approaches to quantify topical drug delivery and tissue distribution have long been preferred to avoid influencing the skin permeation kinetics of the drug by the presence of a conjugated label [31]. While it is possible to quantify the diclofenac content in each skin layer by time-consuming and technically challenging differential extraction and subsequent quantification [32,33], or by open flow microperfusion [34], these methodologies cannot evidence the depth distribution of the drug within the individual tissue layers. This information is critical for establishing the excipient-dependent drug transport, partitioning, and retention in different skin layers, information essential to support the selection of lead formulations during product development. It is also relevant in the fields of skin toxicology and personal safety, e.g., for evaluating the impact of hazards like chemicals pollutants, toxins, occupational irritants or sensitizers, and warfare agents.

Here, we demonstrate the sub-micron visualisation of the tissue distribution and the 24-h kinetics of skin reservoir formation of diclofenac in human skin treated in vitro with a commercial topical pain relief product.

2. Materials and methods

2.1. Skin preparation and dosing

Skin samples were dosed at Charles River Laboratories (CRL), Edinburgh, UK. Samples of full thickness human abdominal skin were from three female donors aged 31 to 67 years from Tissue Solutions Ltd., Glasgow, UK (obtained according to the legal and ethical requirements of the country of collection, with ethical approval and anonymous consent from the donor or nearest relative) [35]. Skin was sourced from Phototype I and II donors to ensure suitability for optical spectroscopy,

since very high melanin content requires imaging at significantly reduced laser powers to prevent otherwise strong absorbance of the light and damage to the skin. The skin was stored at $-20\,^{\circ}\text{C}$ prior to use. Splitthickness skin was prepared using an electric dermatome (Zimmer Ltd., Warsaw, IN, USA) set to a nominal thickness of 400 μm .

The skin was mounted in static Franz diffusion cells (PermeGear Inc., Hellertown, PA, USA) having a nominal receptor chamber volume of 5 mL and a nominal skin exposure area of 0.64 cm 2 . Phosphate buffered saline containing bovine serum albumin (5%, $\ensuremath{w/v}$, as a lipophilic acceptor, and to maintain physiological conditions) was used as the receptor fluid to provide sink conditions and facilitate conventional bulk permeability assessment of the formulations [36]. The receptor fluid was mixed using a magnetic stirrer bar. The diffusion cells were positioned in a manifold heated to maintain a skin surface temperature of 32 \pm 1 $^{\circ}\text{C}$. An electrical resistance barrier integrity assessment was performed and skin samples exhibiting resistance lower than 7.7 k Ω were excluded [37].

Voltaren Forte gel, containing 2.32% diclofenac diethylammonium, and a corresponding placebo gel, were supplied by Haleon CH SARL (the ingredients are listed in Supplementary Information Table S1). The formulations were evenly applied to the stratum corneum surface of the human split-thickness skin membranes using a positive displacement pipette at 0 h of the time course experiment, at a dose of $20~\text{mg/cm}^2$ corresponding to the maximal recommended daily dose of the product.

Three technical replicates were performed for each of the three biological donors, resulting in 9 tissue samples per timepoint of the study, as summarised in Table 1. A full table listing details of each technical and biological replicate number can be found in the Supplementary Information Table S2.

At 4, 8, 16 and 24 h post skin treatment with the Voltaren gel, the corresponding Franz diffusion cell experiments were terminated and 9 total samples (i.e., 3 replicates per donor) were acquired. At 24 h post dose, the 9 skin samples (i.e., controls) exposed to the placebo gel were obtained. Receptor fluid sampling and chemical analysis were also performed. Receptor fluid samples (300 $\mu L)$ were collected only from samples exposed to the Voltaren formulation and were obtained at 0, 4, 8, 16 and 24 h post dose, and then stored in a freezer at $-20~^{\circ} C$. The removed receptor fluid volume was replenished with fresh buffer for cells not terminated.

The receptor fluid samples were analysed by liquid chromatography with tandem mass spectrometry (LC-MS/MS), following a validated procedure. Specifically, LC-MS/MS was performed with an AB Sciex mass spectrometer in turbo ion spray negative mode equipped with a Poroshell EC C-18 column (50 mm \times 2.1 mm, 2.7 µm) which was operated at a flow rate of 500 µL per min. The column temperature was set to 60 $^{\circ}$ C and the autosampler temperature was 4 $^{\circ}$ C. The injection volume was 10 µL. A mixed mobile phase was used: mobile phase A consisted of methanol: formic acid 100:0.5 v/v, and mobile phase B consisted of water: formic acid 100:0.5 v/v. Indomethacin (Sigma Aldrich, Gillingham, UK) was used as an internal standard. Initially 35:65 A:B was applied for min 0 to 1.5, followed by 100:0 A:B for the next 1.5 min, before returning to the 35:65 mixture.

The unexposed skin was cut away from the treated areas, which were then wrapped in aluminium foil, frozen in a freezer at $-80\,^{\circ}\text{C}$, and then finally transferred to and stored in a freezer at $-20\,^{\circ}\text{C}$. The skin samples were transported on dry ice from CRL to the National Physical Laboratory (NPL) where they were stored at $-80\,^{\circ}\text{C}$. The skin discs were sectioned at NPL using a Leica CM 1850 Cryostat (Leica Microsystems, Wetzlar, Germany) at $-20\,^{\circ}\text{C}$. Sections of 30 μm thickness were thawmounted onto glass coverslips (Fisher Scientific, Loughborough, UK), lightly dried under argon gas, vacuum packed, and stored at $-80\,^{\circ}\text{C}$ until analysis. Serial 10 μm thick sections were also generated from each skin sample and used for classical tissue staining with hematoxylin and eosin (H&E); these sections were prepared in the same manner but were instead mounted onto SuperFrost slides (Fisher Scientific, Loughborough, UK).

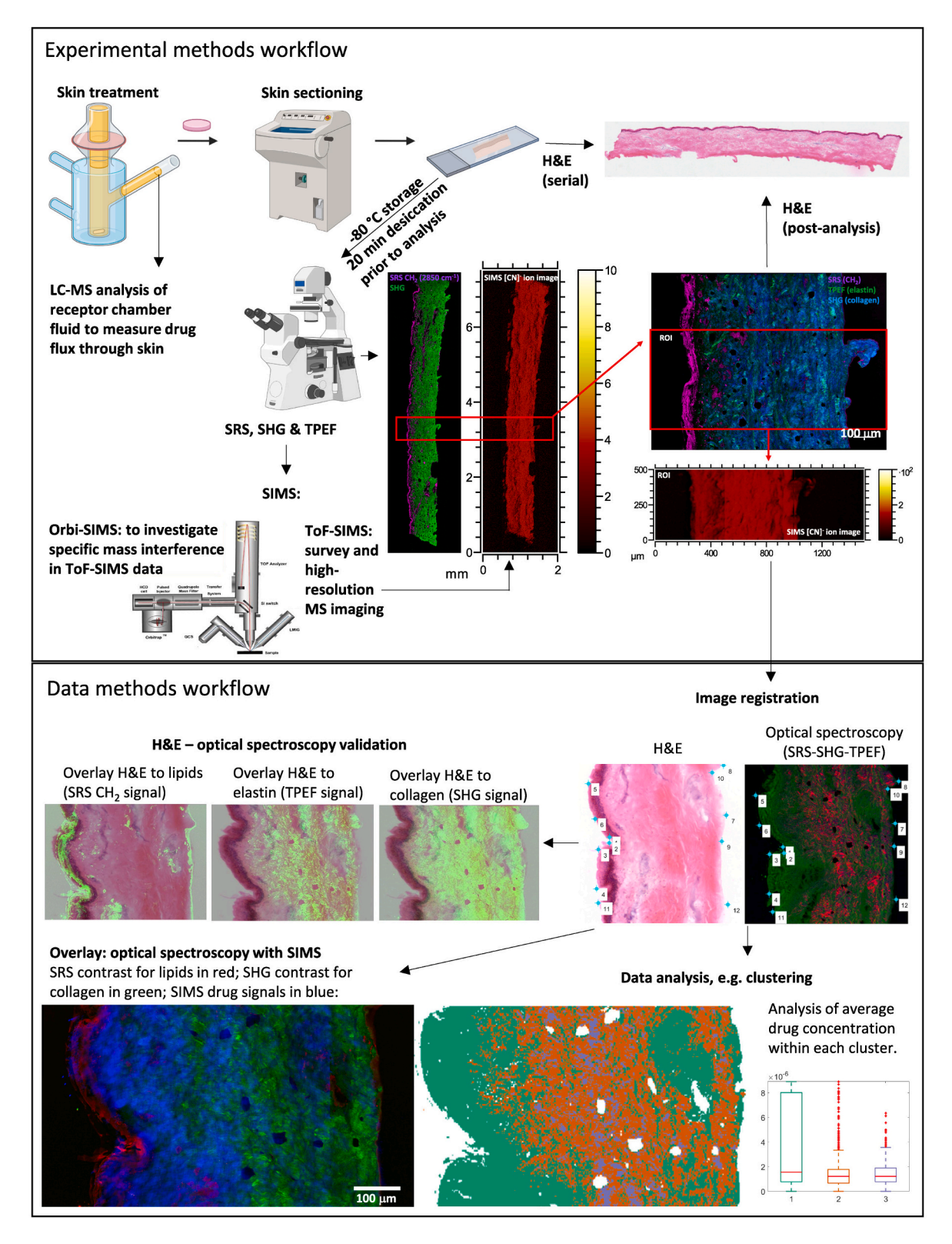


Fig. 1. Method workflow for correlative imaging by optical spectroscopy followed by SIMS. The experimental method workflow comprises skin treatment in a Franz diffusion cell (receptor solution was analysed by LC-MS), followed by sectioning for spectroscopic imaging. Skin sections were analysed by optical spectroscopy (SRS, SHG and TPEF) first, followed by ToF-SIMS. The demonstration for locating the same region of interest within the tissue section is presented for sample 4 which has a hook-shaped protrusion on the dermis side of the tissue section, which was exploited as a convenient marker. The scale bar in the upper SRS-TPEF-SHG image represents 100 μm. In addition to ToF-SIMS, OrbiSIMS was also used to investigate a low-level background mass-interference. H&E staining was performed on the same tissue sections post analysis, in addition to serial sections as a back-up. The data workflow section summarises and presents examples of image registration, and subsequently the generation of overlaid images, including the experimental correlation between optical spectroscopy and ToF-SIMS signals, in addition to validation against physiological structures revealed by H&E staining, and finally cluster analysis, including average drug concentration by cluster. The images presented in the data workflow are of sample 23 (16 h Voltaren-treated). Figure created with BioRender.com.

Table 1Summary of sample numbers and treatments applied.

Sample numbers	Treatment
1–9	4 h with Voltaren gel
10–18	8 h with Voltaren gel
19–27	16 h with Voltaren gel
28-36	24 h with Voltaren gel
37–45	24 h with placebo gel

Veal brain homogenate was used as a quality control (QC) for secondary ion mass spectrometry optimisation. The homogenate was sectioned at a thickness of 30 $\mu m,$ dried as above, mounted onto glass coverslips, and stored at $-80\ ^{\circ} C$ until analysis.

Feasibility studies confirmed that analysis by optical spectroscopy and ToF-SIMS was possible in either order, but each offered some advantages and disadvantages. Optical spectroscopy was carried out at ambient pressure, whereas ToF-SIMS was performed in ultra-high vacuum, and preliminary experiments showed some deformation of the tissue structure due to dehydration of the sample under vacuum. When ToF-SIMS was performed first, the samples were fully dehydrated due to the high vacuum, which made image registration with the optical spectroscopy easier due to less deformation. However, the extreme dehydration resulted in some tissue sections lifting from their glass substrates, which negatively impacted on the optical spectroscopy experiments. Therefore, in this study, non-destructive optical spectroscopy was performed first, followed by ToF-SIMS. The skin and OC samples were desiccated for 30 min under vacuum to remove residual moisture (preventing condensation from forming on the sample surface when warmed to ambient temperature) and to partially dehydrate the sample prior to optical imaging. This step was important to minimise any difference in hydration and, thereby avoid, deformation between the optical spectroscopy and SIMS images acquired under ambient and high vacuum conditions, respectively. This step considerably aided the image registration of the data sets, without risking tissue lifting due to excessive dehydration.

2.2. H&E staining

The H&E staining procedure was based upon the manufacturer's protocol (Shandon Staining Guidance, Thermo Scientific, Loughborough, UK). Slides containing 10- μ m-thick serial sections of skin samples were brought to room temperature under ambient conditions and then fixed in 10% neutral buffered formalin (Sigma Aldrich, Gillingham, UK) for 10 min before they were stained. The full H&E staining protocol is detailed in the Supplementary Information. After clearing, Organo/Limonene Mount (Sigma Aldrich, Gillingham, UK) and glass coverslips were applied to each section in accordance with the manufacturer's protocol. Brightfield optical images of H&E-stained sections were acquired at $10\times$ magnification using a Zeiss Axio Imager M2 (Zeiss, Cambridge, UK).

2.3. Optical spectroscopy

SRS, SHG and TPEF microscopy images were acquired on a Leica SP8 laser scanning microscope (Leica Microsystems, Wetzlar, Germany) coupled to a PicoEmerald-S laser system. The PicoEmerald-S generates two pulsed 2 ps laser beams: a 1031.2 nm Stokes beam which was spatially and temporally overlapped with a tuneable pump beam. The Stokes beam was modulated at 20 MHz and stimulated Raman loss signals were detected using a silicon-based detector and lock-in amplifier (UHFLI, Zurich instruments, Zurich, Switzerland). A second channel was utilised to measure second harmonic and emitted fluorescence signals using a photomultiplier tube. Images were acquired with a water immersion $40\times$ magnification lens (1.1 NA, Leica) used in conjunction with a short working distance air condenser lens (0.9 NA, Leica).

Samples were imaged without a top coverslip, to reduce the risk of disturbing the tissue during removal for subsequent SIMS analysis. The laser power was set to 30% which corresponds to approximately 10 mW for the pump beam and 30 mW for the Stokes beam at the sample.

Detector gain settings were consistently applied across the study with the SRS detector and SHG/fluorescence detectors set to 20 V and 1000 V, respectively, for the C—H stretching regions (2650 cm $^{-1}$, 2850 cm $^{-1}$ and 2945 cm $^{-1}$ for the off-resonance control, CH $_2$ stretching, and CH $_3$ stretching, respectively) and 45 V and 490 V, respectively, for wavenumbers in the fingerprint region (1530 cm $^{-1}$, 1586 cm $^{-1}$ and 1666 cm $^{-1}$ for the off-resonance control, C—C, and Amide *I*, respectively).

Large area mosaic tile scanning was performed using LAS-X 'Navigator' during which 512 \times 512 pixel images were acquired for each tile at X1 zoom with an imaging speed of 400 Hz. For the whole skin section overviews, a line average of 1 was used, whereas for the regions of interest (RoIs), line-averaging of 6 was adopted. The resulting image tiles corresponded to areas of 290 $\mu m \times$ 290 μm and were stitched together using the 'mosaic merge' function in the Leica LAS-X software.

Further image processing steps were performed using ImageJ software (U. S. National Institutes of Health, Bethesda, Maryland, USA, version 1.52a). Where indicated in the text, off-resonance (spurious) SRS signal contributions were subtracted from their on-resonance counterparts in a pixel-by-pixel manner using the 'Image calculator' plugin. Composite SRS-SHG-TPEF images were generated using the 'colour merge' plugin. In addition to the use of consistent instrument and image acquisition parameters, image processing steps have also been consistently applied where signal intensity needed to be directly comparable (e.g., comparison of drug-treated versus placebo-treated tissue signals, or comparison of on- versus off-resonance SRS images).

2.4. Secondary ion mass spectrometry (SIMS)

ToF-SIMS (ToF SIMS 5, IONTOF GmbH, (Muenster, Germany) was performed using a 30 keV Bi₃ primary ion beam with a current of 0.2 pA. All acquisitions were conducted in negative ion polarity, with a 100 ms duty cycle time, a mass range of m/z 0–900, and a beam diameter of 5 μm. A 20 eV electron flood gun at 5 μA was used for charge compensation. SIMS images were acquired immediately following optical spectroscopy acquisition. An overview image was first acquired using the stage macro raster mode to map the entire tissue section with a field of view of 2.5 mm to 3.0 mm \times 8.5 mm to 9.0 mm depending on the tissue dimensions. The overview image was formed from a mosaic of smaller images each with a field of view of 0.5 mm \times 0.5 mm (256 \times 256 pixels) with 1 ion beam shot per pixel giving an ion dose of 8.18×10^8 ions/cm². Images for specific RoIs were acquired using a similar approach with a field of view of 1.0 mm \times 0.5 mm; 4 shots/pixel/frame and 10 frames per patch, corresponding to an ion dose of 1.31×10^{11} ions/cm². For quality control, tissue homogenate samples were analysed immediately prior and after analysis of each skin section. A field of view of 0.5 mm \times 0.5 mm (256 \times 256 pixels) was selected with 1 shot per pixel and 1 frame per scan for a total of 15 scans, for which the ion dose density was 3.27×10^{10} mbar. The resulting mass spectra were calibrated after the acquisition using H⁻, C⁻, C₂ and C₃. Surface Lab 7.1 software was used for the data acquisition and extraction.

High mass resolution analysis was performed using an OrbiSIMS instrument (HybridSIMS, IONTOF GmbH, Muenster, Germany) equipped with an Orbitrap mass spectrometer (Q Exactive HF, Thermo Fisher, Germany). Negative polarity ion mass spectra were acquired with a 20 keV argon gas cluster (Ar $_{3000}^+$) at 20 µm and primary ion beam current of 20.00 pA at 47.73% duty cycle with a 200 µs cycle time. A massresolving power of 240,000 was selected with an injection time of 508 ms, collisional cooling was set in low pressure mode at 4.5×10^{-2} mbar, target potential was adjusted and set at -215 V. The mass range for all the OrbiSIMS acquisition was set at m/z 80–1200. Mass calibration of the Q Exactive HF instrument was performed on the day of

analysis using silver cluster secondary ions. The field of view was 250 $\mu m \times 250~\mu m$ (100 \times 100 pixels). The ion beam used a sawtooth raster pattern, and 50 scans were acquired per mass spectrum. Based on the drug detection, specific areas were selected for high mass resolution imaging using the OrbiSIMS with a beam spot size of $\sim 3~\mu m$. Images were generated by performing a tile mosaic to cover a field of view of 1.5 mm \times 0.5 mm (300 \times 100 pixels). The same raster pattern was used but only 1 scan per pixel was acquired. For all acquisitions, a 20 eV electron flood gun with a current of $-10~\mu A$ was used to compensate for sample charging; this was complemented by Ar gas flooding at a pressure of 7.7 \times 10 $^{-7}$ mbar. Data acquisition was controlled using Surface Lab software version 7.2.125120.

2.5. Approach used to identify same area for correlative imaging

Fig. 1 illustrates the approach used for locating the same RoI for optical spectroscopy followed by ToF-SIMS. First, an SRS large-area tile scan was performed at 2850 cm⁻¹ to reveal the lipid distribution and identify, in particular, the strong signals originating from the stratum corneum; in parallel, second harmonic generation contrast (recorded in a separate channel) revealed the collagen distribution. From the resulting composite image, a RoI was chosen based on the following requirements: (i) it was centrally located, i.e., not within the outer 20% of the sample perimeter that could potentially contain residual un-dosed skin (i.e., the clamped part of the tissue in the Franz cell apparatus); (ii) it was flat enough to be probed within the same optical depth plane; and (iii) it contained a clear structural feature that would aid identification when the sample was transferred to the SIMS setup. For example, in Fig. 1, a 'hook'-shaped protrusion on the dermis side of the section within the selected RoI can be observed in both the optical and ToF-SIMS images. After the RoI was selected using optical spectroscopy, images were obtained from the RoI for all the wavelengths and contrasts described previously. At completion, the sample was removed from the optical microscope and transferred for immediate ToF-SIMS analysis. A similar whole-section image overview was first acquired using SIMS at lower resolution to identify the RoI selected and imaged by optical spectroscopy. This identification was initially performed using visual features, and was then confirmed by calculating the percentage of the RoI distance along the length of the section, compared to the optical spectroscopy image. Once the RoI position had been confirmed, higher resolution SIMS analysis was then performed within the RoI zone acquired using optical spectroscopy, as indicated by the red box within the optical spectroscopy RoI in Fig. 1.

2.6. Image registration & data analysis

Images from SIMS and optical spectroscopy were first reduced to 3 dimensions each using non-negative matrix factorisation [38], to visualise as red, green and blue colour channels as this provides clear identification of different anatomies for the purpose of finding matching features for registration [39,40]. Reduction of the H&E images was not necessary as they were already captured as RGB images. Matching features were then selected using the Matlab control point selection tool "cpselect" (Matlab, Mathworks, 2019b and Image Processing Toolbox), and registration performed using the "cp2tform" and "imtransform" functions using an affine transformation, with the SIMS data used as the fixed images and optical spectroscopy data as the moving images. Examples of registration are shown in Supplementary Information Fig. S1.

ToF-SIMS data for the diclofenac ion images were first normalised to homogenate data collected prior to and after each image acquisition. The average total ion count of the two homogenate datasets (prior and after) was extracted for each matched skin tissue, and the diclofenac intensities in each skin image were divided by this corresponding value. This procedure was performed to account for any changes in instrument response that might occur over the duration of the study, and the data are presented in Supplementary Information Table S4.

Following registration, overlays of the optical spectroscopy and SIMS data were created by setting the respective images as red (SRS image for CH2), green (SHG image for collagen) and blue (SIMS image for diclofenac, comprising signals of several different ions at m/z 214.04, 216.04, 250.02, 252.02, 294.01 and 296.01) channels of an RGB image. A table of the different ions and their assignment is detailed in Supplementary Information Table S5. Overlays of the H&E staining were created by reducing the intensity of the H&E image by a factor of two and adding the corresponding SIMS or optical spectroscopy image to the green channel. This approach was chosen because the H&E images are primarily pink/purple and thus contain high blue and red intensity but little green; the approach therefore achieves the best contrast and preserves maximum information in both modalities. Clustering was then performed on the registered optical spectroscopy data to differentiate the morphological features of the skin using k-means clustering (k = 3, cosine distance) with the Matlab "kmeans" function (Matlab, Mathworks, 2019b and Statistics Toolbox), and the drug ion intensity from the SIMS data was extracted for each cluster. This was then displayed as a boxplot using the Matlab "boxplot" function (Matlab, Mathworks, 2019b and Statistics Toolbox).

Principal component analysis (PCA) was performed on ToF-SIMS data using the Matlab-based application simsMVA (MatLab version 9.8.0.1396136 (R2020a) Update 3 and simsMVA May 2023 version) [41]. The selected treated vs. placebo data sets were integrated into one file, to allow direct comparison and discrimination between the two samples. Poisson scaling was applied to the data and the spectra were mean centred as a pre-processing step. PCA was performed on the mass range m/z 127 to 500 using 64 principal components. The first 6 principal components were selected for analysis. The resulting PCA images were normalised to the overall maximum.

3. Results

3.1. Mapping the skin morphology using optical spectroscopy

SRS microscopy was performed at a range of Raman shifts: 2945 cm $^{-1}$ for CH $_3$ stretching; 2850 cm $^{-1}$ for CH $_2$ stretching; 1666 cm $^{-1}$ for Amide I; and 1586 cm $^{-1}$ for C=C (diclofenac and endogenous species). Two off-resonance controls were acquired at 1530 cm $^{-1}$ and 2650 cm $^{-1}$ for the fingerprint and C—H stretching regions, respectively, to account for differences in detector sensitivity across the wavelength range used [8]. To complement the SRS microscopy, label-free visualisation of the connective tissues was achieved using SHG for collagen and TPEF for elastin. The SHG and TPEF were acquired simultaneously with the SRS imaging in separate channels. Fig. 2 displays an example of label-free images of skin tissue structure obtained by combining SRS with SHG and TPEF microscopies.

To complement the discrete wavenumbers chosen for the imaging, SRS spectra were also acquired for one Voltaren-treated and one placebo-treated sample (Supplementary information, Fig. S2). Although the doublet C=C Raman peaks centred around $1600~{\rm cm}^{-1}$ corresponding to the presence of diclofenac (in treated skin) could be detected in the epidermis, the signal-to-noise ratio was below the limit of detection within the dermal layers of the skin, which motivated the correlative SIMS analysis.

3.2. Mapping the drug distribution within the tissue using SIMS

Diclofenac was observed as a deprotonated ion and its corresponding ³⁷Cl isotope. ToF-SIMS mass spectra of the placebo- vs. Voltaren geltreated tissue are presented in Fig. 3 panel a. Panel b shows ToF-SIMS ion images of Voltaren gel-treated tissue; and signals corresponding to the diclofenac ions can be seen most strongly in the epidermis (left hand edge of the tissue as presented). As can be seen in Fig. 3 panel c, some signals (albeit at a lower intensity) were observed in the placebo-treated sample for the image corresponding to [³⁵ClM-H]⁻, suggestive of a

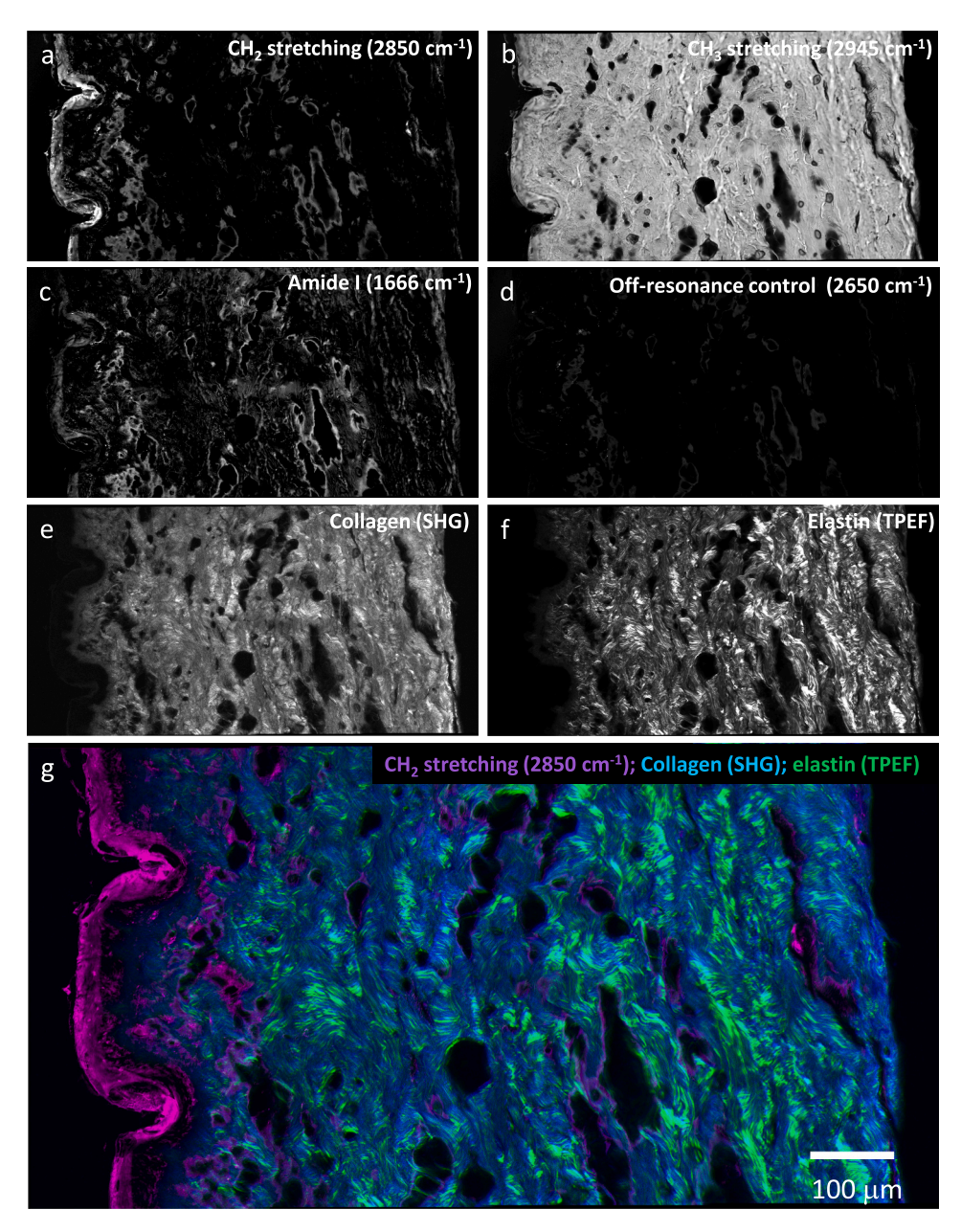


Fig. 2. Optical spectroscopy images for different tissue components. The images presented are of Sample 11 (donor B, Voltaren-treated 8-h timepoint). Panels a) to d) show SRS contrast for CH₂, CH₃, amide I and an off-resonance control respectively. Panels e) and f) show the distribution of collagen from SHG, and elastin from TPEF, respectively. Panel g) presents a composite false-colour image prepared by merging the TPEF signals for elastin in green, SHG for collagen in blue, and SRS signals corresponding to the CH₂ stretching contrast in magenta (the minor off-resonance spurious signal contribution visible in the corresponding image have been subtracted from the CH₂ image using the 'image calculator' plugin in ImageJ prior to generating the composite image).

potential background mass interference. This minor contribution is apparent in the spectrum presented in panel a, which shows a relatively low intensity background signal in the placebo-treated sample at the same m/z as the diclofenac signal (highlighted by the blue dashed rectangles). This was further investigated using high mass-resolution OrbiSIMS [14]. Since Orbitrap MS imaging is considerably more time-intensive than ToF-MS imaging, only one representative product-treated sample and its corresponding placebo-treated sample were selected for an in-depth analysis. A high mass resolution image was acquired from an area where diclofenac was observed: the OrbiSIMS spectrum presented in panel d confirmed with high confidence that most of the signal detected by ToF-SIMS is from diclofenac, and that a minor mass interference was responsible for the weak signals present at the drug ion m/z in the placebo-treated samples. The corresponding Orbi-SIMS images are presented in Supplementary Information Figs. S3–5.

3.3. Application of the new correlative approach to follow the time course of drug tissue distribution after topical application

Although SIMS was demonstrably more sensitive than optical spectroscopy for the detection of diclofenac in the deeper skin layers, visualisation of structural features of the skin was clearer with optical spectroscopy. We therefore applied both techniques to the same tissue samples to obtain both sets of information in a correlative manner. It should be noted that since the optical spectroscopy images were acquired using an inverted microscope, the bottom face of the tissue section (i.e., the one in contact with the glass substrate) was imaged with optical spectroscopy, whereas the top face (i.e., the one at the tissue-air interface) was analysed with SIMS. Therefore, some small structural discrepancies may be expected due to the section thickness being greater than the probe depth of the techniques. The images from SRS and ToF-

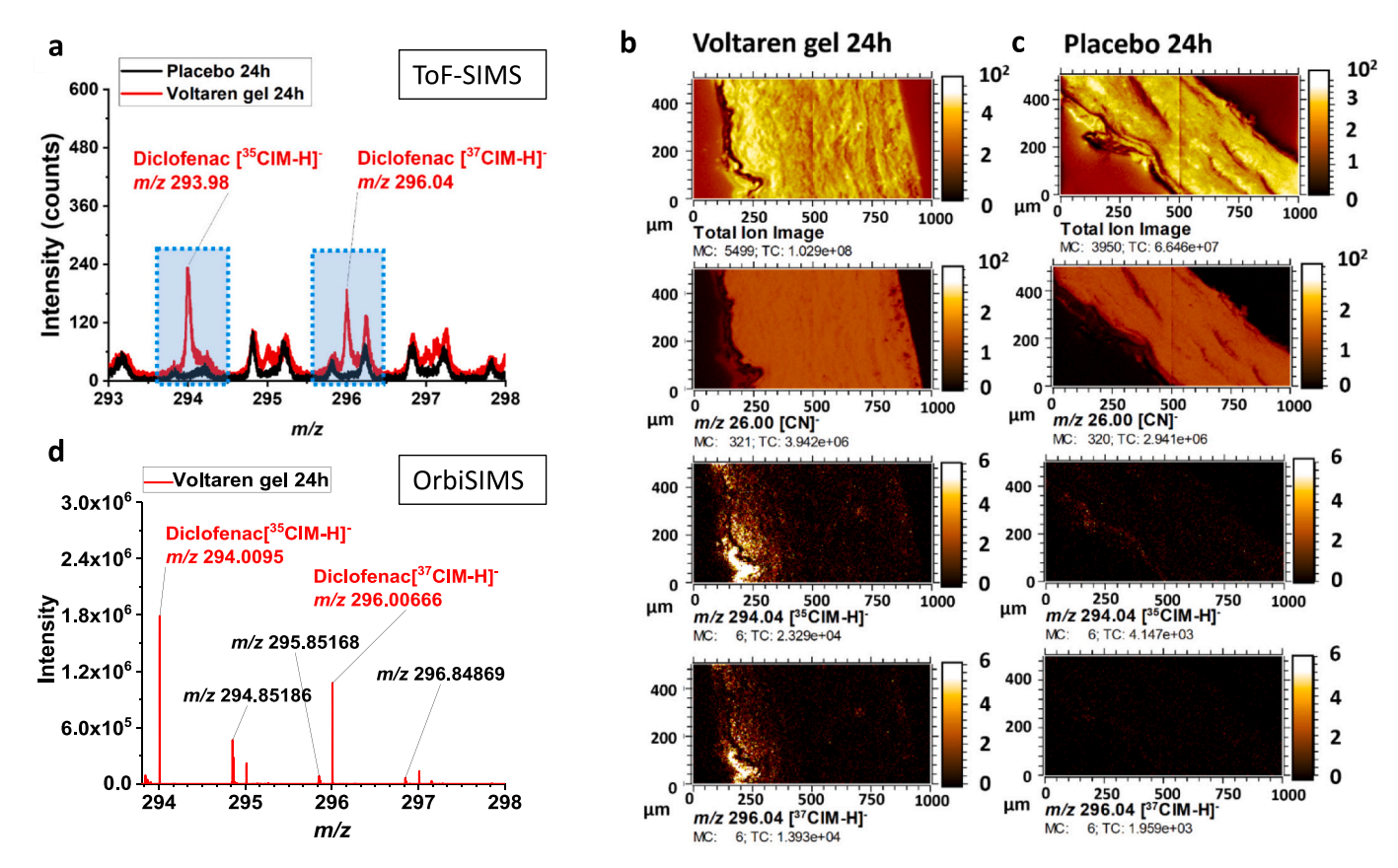


Fig. 3. ToF-SIMS analysis of Voltaren vs. placebo-treated tissue. Panel a shows the ToF-SIMS mass spectra of Voltaren vs. placebo-treated tissue. Panels b and c show the total ion images, [CN]⁻ (corresponding to the CN-containing species from the tissue section) and diclofenac signals as signature ion [³⁵ClM-H]⁻ and [³⁷ClM-H]⁻ for the Voltaren vs. placebo-treated skin samples respectively. Panel d shows a high mass resolution OrbiSIMS spectrum confirming the mass interference. The data presented correspond to samples 32 (24-h Voltaren-treated) and 41 (24-h placebo-treated).

SIMS were registered to the H&E images and overlays were created to show how the features detected in SRS align to the morphological structures in the skin. Examples are shown in the Supplementary Information Fig. S6. All 45 tissue sections (generated by treating excised human skin in vitro with Voltaren or the corresponding placebo formulation during 4, 8, 16, or 24 h as summarised in Table 1 were analysed, and the data sets registered.

Fig. 4 shows the combined registered and merged optical spectroscopy-SIMS images, in which the summed drug intensity signal (from ToF-SIMS measurements) is shown in blue, the lipid-rich tissue structures, in particular the stratum corneum (identified by $\rm CH_2$ stretching contrast at 2850 cm $^{-1}$ using SRS), are shown in red, and the collagen-rich tissue regions (identified by SHG signals) are shown in green. The diclofenac signal from SIMS (blue) comprises signals of several different ions at m/z 214.04, 216.04, 250.02, 252.02, 294.01 and 296.01. This approach provided the best sensitivity and exploited the chlorine isotopes as a confirmatory signal. The SIMS images and further information on these ions can be found in the Supplementary Information (Fig. S7). Note that in Fig. 4, some blue signals are also visible in the placebo-treated tissue sections (far left-hand column). These signals are due to the mass interference discussed previously and confirmed using OrbiSIMS.

As expected, we observed high inter- and intra-donor variability in both the magnitude and the time course of formation of the skin reservoir of diclofenac, reflecting the normal biological variability of the skin barrier [42]. Not surprisingly, the amounts of drug that had permeated through the skin were also highly variable (Supplementary Information Table S3) and did not correlate well with the magnitude of the skin reservoir: R² (the coefficient of determination) for the average SIMS intensity per tissue vs. the cumulative absorption ranged from 0.03 for 4-

h treatment up to 0.32 for 24-h treated skin. This result confirms earlier observations that the two parameters are governed by different factors [43]. While direct analysis of the drug remaining in the skin tissue itself can be performed by tissue extraction and quantification with chemical analysis techniques such as LC-MS/MS, direct spectroscopic imaging such as that presented here provides important advances in spatial information.

Subsequently, the registered optical spectroscopy data from the replicate sets from each donor were clustered using k-means clustering [44] (k = 3, cosine distance metric) and the ToF-SIMS drug ion intensities were extracted from regions of interest defined by each cluster. Fig. 5 shows a representative example (data from donor B, replicate set 2). The skin morphology can be readily differentiated from clustering performed on the optical spectroscopy data, evidencing the power of our untargeted approach to differentiate the skin layers in a manner more advanced than is possible with traditional histological imaging by H&E staining. Analysis of the relative drug intensities across tissue layers clearly revealed a cluster (shown in green in Fig. 5 panel a) in the optical spectroscopy data that coincides primarily with the epidermis in both the Voltaren- and placebo-treated samples. The intensity of all clusters in the product-treated samples collected after longer exposures (16- and 24-h dosing) was higher compared to those at a shorter time (e.g., 4-h), and all were greater than those from the placebo-treated sample for 24 h. Increasing the treatment duration led to a significant increase of the drug amounts retained in the epidermis; after 16-24 h, the drug also was detected in the deep dermis. The intensity of the clusters in the 8-h sample appeared higher than expected (relative to the 16- and 24-h samples); however, in addition to variability between skin samples, this may be explained by this sample being thinner than for the others presented. Since less drug is present in the deeper layers, the average

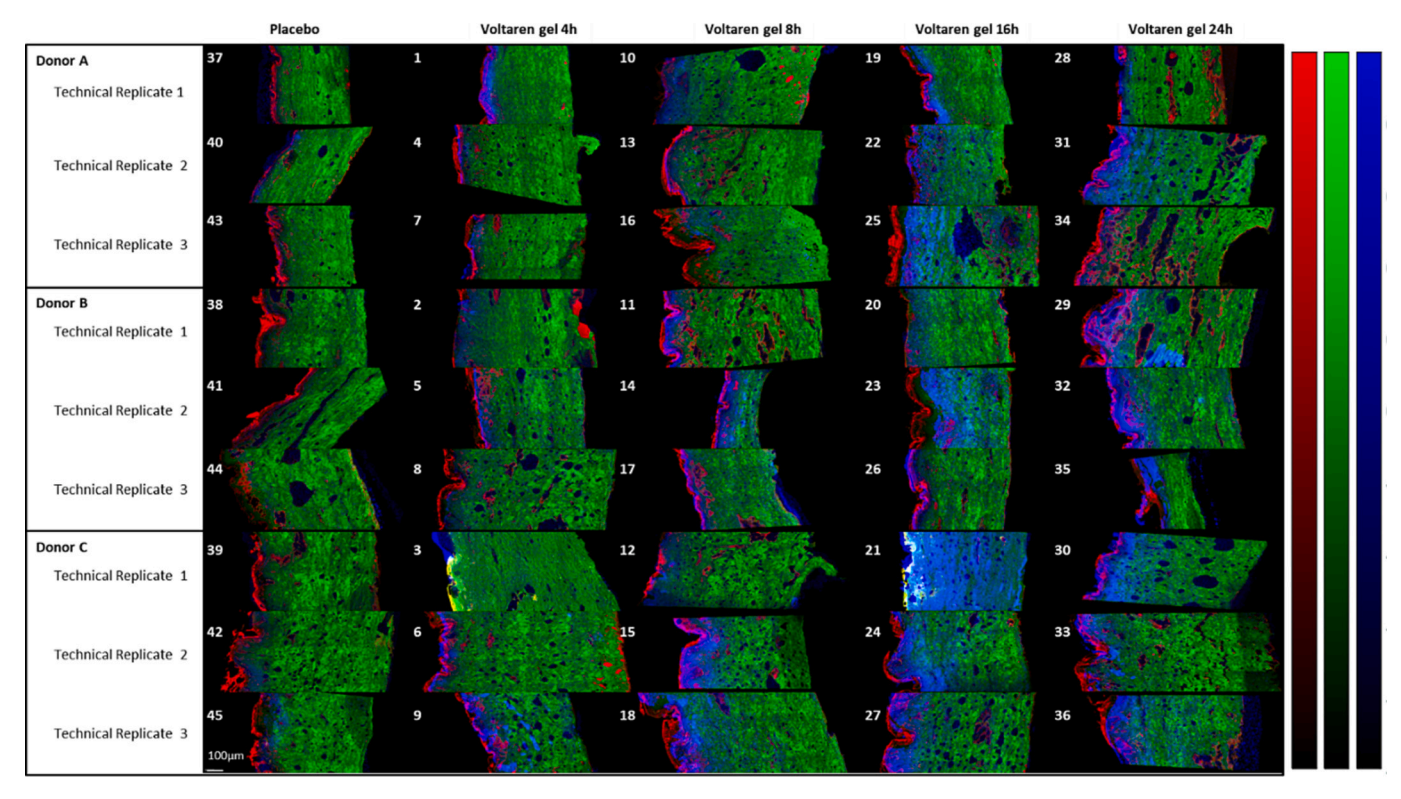


Fig. 4. Overlaid spectroscopic images of the 45 human skin tissue samples. Registered and merged SRS-SHG-SIMS images comprising the lipid distribution from SRS contrast for CH₂ stretching in red, collagen from SHG microscopy in green, and the diclofenac-related signal from SIMS in blue. All images are oriented to display the stratum corneum on the left-hand side. The scale bar (100 μm) for the images is indicated on sample number 45.

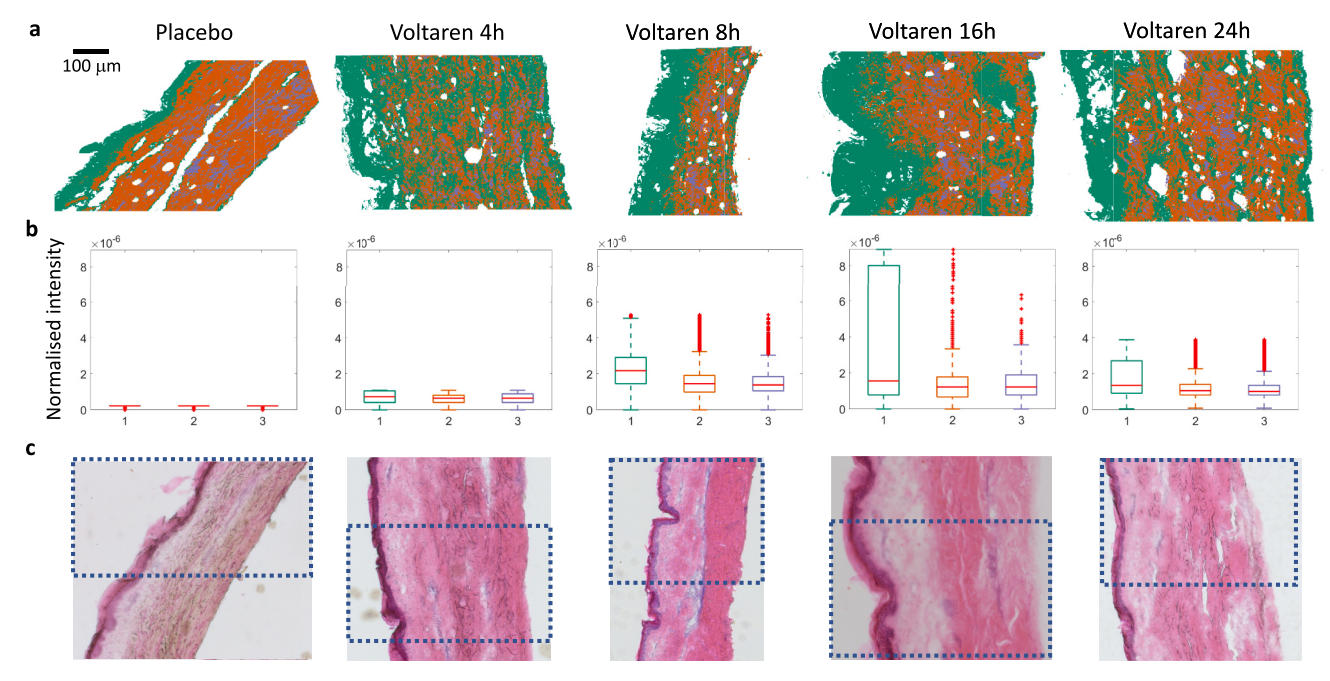


Fig. 5. Clustering approach to differentiate the skin layers. Panel a: Clustering images on the registered optical spectroscopy data. Panel b: the corresponding ToF-SIMS drug ion intensities for the RoI defined by each cluster in the optical images displayed as boxplots (colour scheme matches the clustering in panel a); where the central red line represents the median, the top and bottom of the box represents the 75% and 25% confidence levels respectively, the whiskers represent the range of the 99% confidence level, and any additional points plotted are data points outside those limits. Panel c: corresponding H&E images for the clustering images presented in panel a, with dotted boxes indicating the region of interest analysed. Left to right: skin sections from donor B: 41 (placebo); 5 (4 h); 14 (8 h); 23 (16 h) and 32 (24 h). All images are oriented to display the stratum corneum along the left-hand side of the section.

intensities for the clusters were higher in this thinner piece of skin.

In addition to measuring the penetration of drug into the skin over the time course investigated, there is also a wealth of information in these data regarding endogenous molecules which may localise to specific anatomical regions of the skin or may be co-located with diclofenac. Multivariate analysis can be used to investigate the interactions between all the peaks present within the data in an unsupervised manner. To demonstrate this, PCA was performed on the ToF-SIMS data sets to identify ions that most strongly correlate with the drug distribution. The results are presented in Supplementary Information Fig. S8. PC 1 distinguished the tissue from the substrate (variance 25.55%), PC 2 predominantly distinguished the epidermis from the dermis (variance 7.59%). PC 3 and PC 4 showed selectivity for the drug distribution (the parent ion, and several fragments), with a variance of 6.57% and 5.19% respectively). The drug distribution was correlated with cholesterol sulfate at m/z 465.30, and several other fragments which were predominantly phosphate-based. These species ranged from m/z 127.95 to 180.91 and putatively assigned as $[H_2P_2O_4]^-$; $[P_2O_5H_2]^-$ and [NaP₂O₆]⁻. It should be noted that this analysis will be biased by the relative strength of detection by SIMS, and thus may not reflect the concentrations present.

4. Discussion

This study demonstrates the analytical possibilities of a new, correlative combination of non-linear optical spectroscopic and mass spectrometric imaging. The main advantages of the approach are the considerably higher sensitivity for drug detection (compared to Raman spectroscopy) together with higher (i.e., sub-micron) spatial resolution, and a greater degree of structural information; for example, the connective tissues visualised using SHG and TPEF, compared to previously reported correlative RS-MS studies.

While it has been previously shown that SIMS alone can differentiate the skin layers [25], the correlative use of SRS and SHG offers several advantages. Obtaining a detailed optical image of the tissue prior to SIMS analysis permits the fast identification of regions where the stratum corneum or epidermis is missing, folded over, or defective, which saves repetition of time-intensive measurements. SRS can also identify any drug crystallisation and its phase, which is not possible by SIMS. Similarly, non-destructive multiphoton methods are also able to report on oxidative stress [45], which may be beneficial information for certain formulations/applications. Since these optical methods are performed in ambient conditions, unlike SIMS, they can more easily preserve features or chemistries that are sensitive to high vacuum, e.g., volatile components and delicate structures.

Technical challenges identified included mass interference from endogenous species in the tissue, and topographically induced artefacts in non-flat samples, which was overcome by selecting regions that were well adhered to the substrate and optimal for analysis by both techniques. Additional challenges that may be relevant to the application of this methodology to other sample types include orientation issues, e.g., polarization-dependent Raman signals, and for tissue types with less clearly identifiable features, the use of fiducial markers may be necessary to locate the same RoI.

Future opportunities to advance this approach include data fusion [46], automated image correlation [47], and 3D correlative analysis (since both SIMS and optical spectroscopy can be performed in 3D by sputtering and optical sectioning, respectively) [48]. Correlative analysis between optical spectroscopy and SIMS may also be important to better understand each respective technique; for example, to explain signal non-linearity with concentration, or to study artefacts. However, care is required when interpreting the two datasets, since the techniques probe different information depths: the depth resolution of SIMS is significantly smaller (typically a few nm) compared to that of SRS microscopy which is approximately 1 μ m. Both techniques can acquire 3D data sets, however SIMS is limited by the practicality of time and

topography artefacts when sputtering away incremental layers of material. The optical spectroscopy methods are limited to probing a few tens to a few hundred microns into the skin, due to increasing signal loss with depth, caused by scattering and absorption of light by the tissue. Another potential application of the correlative approach would be the use of optical spectroscopy to screen large tissue sections rapidly for more detailed, subsequent investigation of smaller RoIs by SIMS, which is more time intensive. Further, while SIMS can only be performed in vitro, the rich information it provides can nevertheless offer important insight into complex Raman signals and better inform, therefore, the in vivo application of RS and SRS microscopy.

5. Conclusion

In conclusion, this study has successfully applied correlative methodology to human skin samples treated in vitro with a commercial topical product to visualise drug reservoir formation with unprecedented spatial resolution and chemical sensitivity. The data demonstrated that initially (4-8 h post-treatment), the drug reservoir built up primarily in the epidermis; later (16-24 h post-treatment), it expanded considerably in size and into the deep dermis. In line with the highly variable skin permeation of diclofenac, the reservoir displayed large inter- and intra-donor variability. In the field of topical pharmaceutical product development, therefore, this approach has the potential to identify lead candidates capable of creating significant drug reservoirs in the skin and thereby ensuring prolonged therapeutic action; of course, the technique can also address the reverse question of drug clearance, i. e., the time course of reservoir depletion. In addition, this new correlative method is applicable to other soft tissues (originating from in vitro or clinical studies) including, but not limited to, oral epithelia, gut mucosa, or muscle, and for biodistribution studies in which a sufficiently sensitive method is needed to follow drugs or harmful chemicals to their site of intended therapeutic action or toxicity.

Author contributions

The study was designed by NAB, CN, EG, RHG and MBB. Skin dosing and Franz diffusion cell chemical analysis was performed at Charles River Laboratories by LP. The remaining experimental work was performed at the National Physical Laboratory. Skin sectioning was performed by CN; H&E staining was performed by CN and DT. Optical spectroscopy was performed by DT and NAB; ToF-SIMS analysis was performed by JLV, MVT and JZ. OrbiSIMS was performed by JLV. ISG provided advice and oversight of ToF-SIMS and OrbiSIMS data and interpretation. Image registration and cluster analysis was performed by AD and TM, PCA was performed by JLV and GFT. The manuscript was written by NAB, AD, JLV, CN and MBB, and was reviewed by, and appropriately amended by, all authors.

CRediT authorship contribution statement

Natalie A. Belsey: Supervision, Project administration, Methodology, Investigation, Funding acquisition, Conceptualization, Writing - original draft, Writing - review & editing. Alex Dexter: Writing - review & editing, Writing - original draft, Visualization, Software, Methodology, Formal analysis. Jean-Luc Vorng: Writing - review & editing, Writing - original draft, Methodology, Investigation. Dimitrios Tsikritsis: Writing - review & editing, Methodology, Investigation. Chelsea J. Nikula: Methodology, Investigation, Writing - original draft, Writing review & editing. Teresa Murta: Visualization, Software, Methodology, Formal analysis. Maria-Vitalia Tiddia: Writing - review & editing, Investigation. Elzbieta Gurdak: Writing - review & editing, Supervision, Project administration. Gustavo F. Trindade: Writing - review & editing, Software, Formal analysis. Ian S. Gilmore: Writing - review & editing, Supervision. Leanne Page: Writing - review & editing, Methodology,

Investigation. Clive S. Roper: Writing – review & editing, Methodology, Conceptualization. Richard H. Guy: Methodology, Conceptualization, Funding acquisition, Writing – review & editing. Mila Boncheva Bettex: Writing – review & editing, Writing – original draft, Supervision, Project administration, Methodology, Funding acquisition, Conceptualization.

Declaration of Competing Interest

This work was funded by Haleon CH SARL. CR is currently a consultant for Haleon CH SARL but was employed at CRL at the time of this work.

Data availability

The data that has been used is confidential.

Acknowledgements

The authors are grateful to Alex Shard (NPL) and David Moore (Omero Consulting Ltd) for helpful discussions, and to Marcel Niehaus (formerly NPL) for the preparation of yeal brain homogenate.

This work was funded by Haleon CH SARL. The contributions of NAB and RHG were supported in part by the Food and Drug Administration (FDA) of the U.S. Department of Health and Human Services (HHS) as part of a financial assistance award (1-U01-FD006533). The contents of this article are those of the authors and do not necessarily represent the official views of, nor an endorsement by, FDA/HHS or the U.S. Government. Support by the Community for Analytical Measurement Science is also gratefully acknowledged for a 2020 CAMS Fellowship Award to Natalie Belsey funded by the Analytical Chemistry Trust Fund.

Appendix A. Supplementary data

Supplementary data to this article can be found online at https://doi.org/10.1016/j.jconrel.2023.10.026.

References

- [1] C.V. Raman, K.S. Krishnan, A new type of secondary radiation, Nature 121 (3048) (1928) 501–502.
- [2] R.L. McCreery, Raman Spectroscopy for Chemical Analysis, John Wiley & Sons, Inc., 2000.
- [3] Q.A.-O. Zhang, et al., Visualization of epidermal reservoir formation from topical diclofenac gels by Raman spectroscopy, J. Pain Res. 13 (1621–1627) (2020).
- [4] G.P.S. Smith, et al., Raman imaging of drug delivery systems, Adv. Drug Deliv. Rev. 89 (2015) 21–41.
- [5] L. Franzen, M. Windbergs, Applications of Raman spectroscopy in skin research from skin physiology and diagnosis up to risk assessment and dermal drug delivery, Adv. Drug Deliv. Rev. 89 (2015) 91–104.
- [6] W. Freudiger Christian, et al., Label-free biomedical imaging with high sensitivity by stimulated Raman scattering microscopy, Science 322 (5909) (2008) 1857–1861.
- [7] W.M. Ji-Xin Cheng, Yasuyuki Ozeki, Dario Polli, Stimulated Raman Scattering Microscopy Techniques and Applications, Elsevier, 2021.
- [8] D. Tsikritsis, E.J. Legge, N.A. Belsey, Practical considerations for quantitative and reproducible measurements with stimulated Raman scattering microscopy, Analyst 147 (21) (2022) 4642–4656.
- [9] N.A. Belsey, et al., Evaluation of drug delivery to intact and porated skin by coherent Raman scattering and fluorescence microscopies, J. Control. Release 174 (2014) 37–42.
- [10] B. Sarri, et al., Stimulated Raman Histology: One to One Comparison with Standard Hematoxylin and Eosin Staining, Biomed. Opt. Express 10 (2019) 5378–5384.
- [11] M. Lee, et al., Recent advances in the use of stimulated Raman scattering in histopathology, Analyst 146 (3) (2021) 789–802.
- [12] J. Mansfield, et al., Chemically specific imaging and in-situ chemical analysis of articular cartilage with stimulated Raman scattering, J. Biophotonics 6 (10) (2013) 803–814.
- [13] A.R. Buchberger, et al., Mass spectrometry imaging: a review of emerging advancements and future insights, Anal. Chem. 90 (1) (2018) 240–265.

- [14] M.K. Passarelli, et al., The 3D OrbiSIMS—label-free metabolic imaging with subcellular lateral resolution and high mass-resolving power, Nat. Methods 14 (12) (2017) 1175–1183.
- [15] M. Fujii, et al., Study on the detection limits of a new argon gas cluster ion beam secondary ion mass spectrometry apparatus using lipid compound samples, Rapid Commun. Mass Spectrom. 28 (8) (2014) 917–920.
- [16] M. Lagator, et al., Sensitivity enhancement using chemically reactive gas cluster ion beams in secondary ion mass spectrometry (SIMS), Surf. Interface Anal. 54 (4) (2022) 349–355.
- [17] S. Sheraz, et al., Enhanced ion yields using high energy water cluster beams for secondary ion mass spectrometry analysis and imaging, Anal. Chem. 91 (14) (2019) 9058–9068.
- [18] M.K. Passarelli, et al., Single-cell analysis: visualizing pharmaceutical and metabolite uptake in cells with label-free 3D mass spectrometry imaging, Anal. Chem. 87 (13) (2015) 6696–6702.
- [19] A. Brunelle, O. Laprévote, Recent Advances in Biological Tissue Imaging with Time-of-Flight Secondary Ion Mass Spectrometry: Polyatomic Ion Sources, Sample Preparation, and Applications, Curr. Pharm. Des. 13 (32) (2007) 3335–3343.
- [20] D. Touboul, A. Brunelle, O. Laprévote, Mass spectrometry imaging: towards a lipid microscope? Biochimie 93 (1) (2011) 113–119.
- [21] P. Massonnet, R.M.A. Heeren, A concise tutorial review of TOF-SIMS based molecular and cellular imaging, J. Anal. At. Spectrom. 34 (11) (2019) 2217–2228.
- [22] D. Schaumlöffel, Secondary ion mass spectrometry for biological applications, J. Anal. At. Spectrom. 35 (6) (2020) 1045–1046.
- [23] P. Sjövall, et al., Imaging of distribution of topically applied drug molecules in mouse skin by combination of time-of-flight secondary ion mass spectrometry and scanning Electron microscopy, Anal. Chem. 86 (7) (2014) 3443–3452.
- [24] N.J. Starr, et al., Elucidating the molecular landscape of the stratum corneum, Proc. Natl. Acad. Sci. 119 (12) (2022), e2114380119.
- [25] P. Sjövall, et al., Imaging the distribution of skin lipids and topically applied compounds in human skin using mass spectrometry, Sci. Rep. 8 (1) (2018) 16683.
- [26] R. Masyuko, et al., Correlated imaging a grand challenge in chemical analysis, Analyst 138 (7) (2013) 1924–1939.
- [27] T.W. Bocklitz, et al., Deeper understanding of biological tissue: quantitative correlation of MALDI-TOF and Raman imaging, Anal. Chem. 85 (22) (2013) 10829–10834.
- [28] O. Ryabchykov, J. Popp, T. Bocklitz, Fusion of MALDI spectrometric imaging and Raman spectroscopic data for the analysis of biological samples, Front. Chem. (2018) 6.
- [29] D.R. Ahlf, et al., Correlated mass spectrometry imaging and confocal Raman microscopy for studies of three-dimensional cell culture sections, Analyst 139 (18) (2014) 4578–4585.
- [30] E.C. Randall, et al., Integrated mapping of pharmacokinetics and pharmacodynamics in a patient-derived xenograft model of glioblastoma, Nat. Commun. 9 (1) (2018) 4904.
- [31] R.O. Potts, R.H. Guy, Predicting Skin Permeability, Pharm. Res. 9 (5) (1992) 663–669.
- [32] J. Pradal, Comparison of skin permeation and putative anti-inflammatory activity of commercially available topical products containing ibuprofen and diclofenac, J. Pain Res. 13 (2020) 2805–2814.
- [33] J. Pradal, et al., Importance of the formulation in the skin delivery of topical diclofenac: not all topical diclofenac formulations are the same, J. Pain Res. 12 (1149–1154) (2019).
- [34] J. Hummer, et al., Optimization of topical formulations using a combination of in vitro methods to quantify the transdermal passive diffusion of drugs, Int. J. Pharm. 620 (2022), 121737.
- [35] Tissue Solutions, 11th August. Available from: https://www.tissue-solutions.com/about-us/our-ethics/, 2022.
- [36] OECD, Test No. 428: skin absorption: in vitro method, in: OECD Guidelines for the Testing of Chemicals, Section 4, 2004.
- [37] S. Whitson, Creation of New Barrier Integrity Rejection Criteria Using Historical Data, 2020. Charles River Study No. 996419.
- [38] X.-C. Xiong, et al., Feature extraction approach for mass spectrometry imaging data using non-negative matrix factorization, Chin. J. Anal. Chem. 40 (5) (2012) 663-669
- [39] J.M. Fonville, et al., Hyperspectral visualization of mass spectrometry imaging data, Anal. Chem. 85 (3) (2013) 1415–1423.
- [40] W.M. Abdelmoula, et al., Automatic generic registration of mass spectrometry imaging data to histology using nonlinear stochastic embedding, Anal. Chem. 86 (18) (2014) 9204–9211.
- [41] G.F. Trindade, M.-L. Abel, J.F. Watts, simsMVA: a tool for multivariate analysis of ToF-SIMS datasets, Chemom. Intell. Lab. Syst. 182 (2018) 180–187.
- [42] V.M. Meidan, C.S. Roper, Inter- and intra-individual variability in human skin barrier function: a large scale retrospective study, Toxicol. in Vitro 22 (4) (2008) 1062–1069.
- [43] M. Hagen, M. Baker, Skin Penetration and Tissue Permeation After Topical Administration of Diclofenac, Curr. Med. Res. Opin. 33 (9) (2017) 1623–1634.
- [44] A. Dexter, et al., Testing for multivariate normality in mass spectrometry imaging data: a robust statistical approach for clustering evaluation and the generation of synthetic mass spectrometry imaging data sets, Anal. Chem. 88 (22) (2016) 10893–10899.

- [45] K.M. Hanson, R.M. Clegg, Observation and Quantification of Ultraviolet-Induced Reactive Oxygen Species in Ex Vivo Human Skin, Photochem. Photobiol. 76 (1) (2002) 57–63.
- [46] A.M. Race, et al., Correlative hyperspectral imaging using a dimensionality-reduction-based image fusion method, Anal. Chem. 92 (16) (2020) 10979–10988.
- [47] T.G. Schaaff, P.J. McMahon, Jm Fau-Todd, P.J. Todd, Semiautomated Analytical
- Image Correlation, Anal. Chem. 74 (17) (2002) 4361–4369.

 [48] K. Dreisewerd, J.Y. Yew, Mass spectrometry imaging goes three dimensional, Nat. Methods 14 (12) (2017) 1139–1140.